

# Chasing Down the $\text{Eu}^{2+}$ Ions: The Delicate Structure–Property Relationships in the Ultra-Narrow Band Phosphor $\text{K}_{1.6}\text{Na}_{2.1}\text{Li}_{0.3}[\text{Li}_3\text{SiO}_4]_4:\text{Eu}^{2+}$

Freia Ruegenberg, Amador García-Fuente, Markus Seibald, Dominik Baumann, Simon Peschke, Werner Urland, Andries Meijerink, Hubert Huppertz, and Markus Suta\*


$\text{Eu}^{2+}$ -activated phosphors of the  $\text{UCr}_4\text{C}_4$  structure type have emerged as promising new (ultra-)narrow band phosphors. Especially the  $\text{UCr}_4\text{C}_4$ -type alkali lithosilicates have caused a sensation in the field of phosphor research in the recent years due to their consistent (ultra)narrow-band luminescence in the cyan and green range that can pave the way to novel backlighting LEDs with high color gamut. The compound “ $\text{K}_2\text{Na}_2[\text{Li}_3\text{SiO}_4]_4:\text{Eu}^{2+}$ ” stands out with a strikingly narrow emission in the cyan range ( $<0.2$  eV or  $<30$  nm full width at half maximum in the energy or wavelength scale, respectively) but the position of the  $\text{Eu}^{2+}$  ions within this structure has been so far controversial. High-resolution photoluminescence spectroscopy at 10 K reveals a complex emission spectrum with seven emission bands in the violet to green range. Combination with single-crystal X-ray diffraction (SCXRD) demonstrates that the cation channels in the structure also contain  $\text{Li}^+$  ions. The presence of emission bands in the violet and blue spectral range reveals that the  $\text{Eu}^{2+}$  ions also occupy the available K sites in the structure independently confirmed by advanced ligand field calculations. This study demonstrates that a combination of SCXRD, photoluminescence spectroscopy, and theory can help elucidate advanced structural problems.

## 1. Introduction

The constant drive for further improvement of LED-based lighting systems has literally led to a race for new phosphor materials in the past years.<sup>[1–11]</sup> Narrow band emitters have become particularly important in that area as they allow to achieve high color purity and maximum accessible color gamut, which are mandatory for a high luminous efficacy based on a reduction of losses in areas of low eye sensitivity.<sup>[7,12–19]</sup> Especially  $\text{Eu}^{2+}$  has gained considerable attraction as an emitter in inorganic phosphors. This is related to its electric dipole-allowed  $4f^7 \leftrightarrow 4f^65d^1$  transition typically located in the visible range that allows to efficiently excite  $\text{Eu}^{2+}$  ions without significant droop at high incident flux.<sup>[20]</sup> Moreover, the energy of this type of transition can be tuned in a controllable manner by appropriate choice of the crystalline surrounding host compound. It has

F. Ruegenberg, H. Huppertz  
Institute of General  
Inorganic and Theoretical Chemistry  
University of Innsbruck  
Innrain 80-82, Innsbruck 6020, Austria

A. García-Fuente  
Department of Physics  
University of Oviedo  
Oviedo E-33007, Spain  
A. García-Fuente  
Nanomaterials and Nanotechnology Research Center CINN  
CISC-University of Oviedo  
El Entegro E-33424, Spain

 The ORCID identification number(s) for the author(s) of this article can be found under <https://doi.org/10.1002/adom.202101643>.

© 2021 The Authors. Advanced Optical Materials published by Wiley-VCH GmbH. This is an open access article under the terms of the Creative Commons Attribution-NonCommercial-NoDerivs License, which permits use and distribution in any medium, provided the original work is properly cited, the use is non-commercial and no modifications or adaptations are made.

DOI: 10.1002/adom.202101643

M. Seibald, D. Baumann, S. Peschke  
OSRAM Opto Semiconductors GmbH  
Mittelstetter Weg 2, 86830 Schwabmünchen, Germany

W. Urland  
Private Institute of Theoretical Chemical Physics  
Muralto 6600, Switzerland

A. Meijerink, M. Suta  
Condensed Matter & Interfaces  
Debye Institute for Nanomaterials Sciences  
Department of Chemistry  
Utrecht University  
Princetonplein 1, Utrecht 3584 CC, The Netherlands

M. Suta  
Inorganic Photoactive Materials  
Institute of Inorganic Chemistry  
Heinrich Heine University Düsseldorf  
Universitätsstraße 1, 40225 Düsseldorf, Germany  
E-mail: markus.suta@hhu.de

been elucidated that a rigid, highly cross-linked crystal structure of the host induces ultra-narrow  $4f^65d^1 \rightarrow 4f^7$  emission bands (ultra-narrow: full width at half maximum (fwhm) of  $<0.2$  eV) of the incorporated  $\text{Eu}^{2+}$  ions, especially for a highly symmetric first coordination sphere.<sup>[21]</sup> Such a structural feature is also typically connected to high thermal quenching temperatures and is realized in nitridosilicates such as  $\text{M}_2\text{Si}_5\text{N}_8$  ( $\text{M} = \text{Sr}, \text{Ba}$ ) with a condensed network of corner-sharing  $[\text{SiN}_4]$ -tetrahedra, representing suitable candidates for phosphor materials.<sup>[1,7,22–24]</sup> The structural extension of the anionic framework with oxide and incorporation of  $\text{Li}^+$  and  $\text{Al}^{3+}$  as additional network builders extend this material class to the oxidonitridosilicates and oxidonitridoalumosilicates such as  $\beta\text{-SiAlON}$ ,<sup>[12,25,26]</sup>  $\text{MSi}_2\text{O}_2\text{N}_2$  ( $\text{M} = \text{Ca}, \text{Sr}, \text{Ba}, \text{Eu}$ ),<sup>[27–35]</sup> or  $\text{Sr}[\text{Li}_2\text{Al}_2\text{O}_2\text{N}_2]$  (SALON),<sup>[13]</sup> in which the  $4f^65d^1 \rightarrow 4f^7$  transition of doped  $\text{Eu}^{2+}$  ions is also characterized by (ultra) narrow emission bands. As a consequence of the layered structure and the various possibilities for order/disorder effects, many in-depth structural investigations were performed on the so-called “2-2-2” oxidonitridosilicates  $\text{MSi}_2\text{O}_2\text{N}_2$  to correlate the manifold structural information to the unambiguous describable photoluminescence properties of incorporated  $\text{Eu}^{2+}$  ions into these materials. Another particularly ultra-narrow band emission is observed in the  $\text{Eu}^{2+}$ -activated nitridolithoaluminate  $\text{Sr}[\text{LiAl}_3\text{N}_4]$  (SLA) at 650 nm close to the edge of the eye sensitivity curve with only 50 nm ( $1180 \text{ cm}^{-1}$ ) fwhm.<sup>[7]</sup> It has similar structural motifs to the previously mentioned compounds and crystallizes in a so-called  $\text{UCr}_4\text{C}_4$  structure type. Most of these compounds show typical orange to red emission due to the soft, polarizable nature of the surrounding  $\text{N}^{3-}$  ions that make the  $\text{Eu-N}$  bonds particularly covalent and lead to a low energy of the excited  $4f^65d^1$  barycenter by means of the nephelauxetic effect. This structure-property relationship led to the success of nitrido(lithoalumo)silicates as red components for phosphor-converted white light LEDs. Only selected hydrides<sup>[36,37]</sup> and sulfides<sup>[38,39]</sup> were conclusively demonstrated to even emit in the lower energetic near-infrared range upon activation with  $\text{Eu}^{2+}$ .

Despite their structural parallels to the nitridoalumosilicates, alkali lithosilicates have not been in the focus of phosphor research for a long time. A reason why they might have not been initially considered as a host material was presumably the fact that the structure built from monovalent cations was considered unsuitable for doping with strongly absorbing higher valent activator ions with electric dipole-allowed  $4f^n \rightarrow 4f^{n-1}5d^1$  transitions such as  $\text{Eu}^{2+}$  ( $n = 7$ ) or  $\text{Ce}^{3+}$  ( $n = 1$ ).<sup>[40]</sup> However, already in the 1980s, Hoppe’s research group was able to synthesize several representatives and examined the substance class in detail.<sup>[41–45]</sup> Their structure partially also derives from the previously mentioned  $\text{UCr}_4\text{C}_4$  aristotype. The fully oxide-based network structure in the host compound and the more ionic nature of the  $\text{Eu-O}$  bond expectedly allows to shift the respective emission wavelengths towards the cyan range compared to the (oxido)nitridolithoalumosilicates. For this wavelength range, finding efficient candidates with low thermal quenching for narrow band emitters still poses challenges.<sup>[40]</sup> This wavelength range is of high interest for, for example, human-centric lighting LEDs that affect the melatonin production within the body and thus have an influence on the circadian rhythm. One potential material class formally fulfilling the

requirements for efficient cyan-emitting phosphors are  $\text{Eu}^{2+}$ -activated oxido(nitrido)beryllates  $\text{AELi}_2[\text{Be}_4\text{O}_6]$  ( $\text{AE} = \text{Sr}, \text{Ba}$ ) and  $\text{Sr}[\text{Be}_6\text{ON}_4]$ ,<sup>[46,47]</sup> or the highly condensed nitridoberyllates  $\text{AEBe}_{20}\text{N}_{14}$  ( $\text{AE} = \text{Sr}, \text{Ba}$ )<sup>[48,49]</sup> but the Be-related toxicity limits their application.

It was not until 2018 that the first publications of  $\text{Eu}^{2+}$ -doped alkali lithosilicates appeared and opened a whole new research field on this substance class.<sup>[50–55]</sup> Especially the groups led by Huppertz, Xia, or Liu established the material class of luminescent alkali lithosilicates by constant extension of new representatives.<sup>[21,51–66]</sup>

The success of this phosphor class for efficient ultra-narrow band emission in the cyan gap has led to a significant increase in publications about new representatives in the last three years. Fundamental questions about the actual position of the  $\text{Eu}^{2+}$  ions in these hosts have remained speculative, however. A resolution of the activator ion position by single-crystal X-ray diffraction (SCXRD) is indeed possible in special cases, but often the dopant is present directly on a metal ion position, on which it gives only an insignificant contribution to the X-ray scattering density. Especially for alkali lithosilicates with several alkali ions, an answer to the question of the activator site is essential for the investigation and understanding of structure-property relationships and targeted design of the emission color and band width of  $\text{Eu}^{2+}$  in such compounds. For that purpose, we selected the ambiguous example of “ $\text{K}_2\text{Na}_2[\text{Li}_3\text{SiO}_4]_4:\text{Eu}^{2+}$ ” ( $\text{KNLLSO}:\text{Eu}^{2+}$ ), which supposedly shows mixed occupation concerning parts of the  $\text{K}^+$  and  $\text{Na}^+$  as well as the  $\text{Na}^+$  and  $\text{Li}^+$  ions. Especially the exact position of the  $\text{Li}^+$  ions is so far ambiguous as structure refinements from averaged powder X-ray diffraction (PXRD) data led to the conclusion of sole presence of the  $\text{Li}^+$  ions in the  $[\text{LiO}_4]$  tetrahedra in the network backbone and not within the present cube-like cation coordination polyhedra.<sup>[61]</sup> However, as has been elucidated from earlier studies,  $\text{Eu}^{2+}$  does have the possibility to substitute  $\text{K}^+$  (only demonstrated in fluorido or hydridoperovskites),<sup>[67–72]</sup>  $\text{Na}^+$ ,<sup>[58,59]</sup> or even occupy vacancies between Li sites,<sup>[21]</sup> which expectedly gives rise to a very complicated emission spectrum and has so far only been controversially discussed in  $\text{KNLLSO}:\text{Eu}^{2+}$ .<sup>[61,73]</sup> Combined analysis by SCXRD for structural resolution as well as high-resolution luminescence spectroscopy at liquid He temperatures ( $T \approx 10$  K) together with time-resolved luminescence helps establish the desirable structure-property relationships that would allow to target the width and wavelength of the  $\text{Eu}^{2+}$ -related emission in these compounds. For this type of investigation, it is relevant to use low doping concentrations to avoid any potential interactions between different  $\text{Eu}^{2+}$  and to avoid inhomogeneous broadening. The spectroscopic assignment was independently supported by ligand field calculations based on a multi-electronic Hamiltonian parametrized from density functional theory (DFT) simulations, which have been recently shown to have the potential to predict the emission and absorption wavelengths of the otherwise computationally very demanding  $\text{Eu}^{2+}$  ions even in low symmetries.<sup>[74–77]</sup> With this uncommon combination of detailed structural, spectroscopic, and theoretical investigations, we aim at giving a more enlightening picture of the site occupation of the  $\text{Eu}^{2+}$  ions in the emerging class of alkali lithosilicate phosphors using  $\text{KNLLSO}:\text{Eu}^{2+}$  as a representative example.

## 2. Results and Discussion

### 2.1. Structural Classification

The variations among the different alkali lithosilicates can be all traced back to the aristotype of  $\text{UCr}_4\text{C}_4$ . Structurally, they thus show significant analogies. An unambiguous categorization is possible based on their space group. The basic structure of all described substances is built from a rigid anionic framework of corner- and edge-sharing  $[\text{LiO}_4]$ - and  $[\text{SiO}_4]$ -tetrahedra. One characteristic feature is the formation of *vierer-ring* channels<sup>[78]</sup> in the lithosilicate structure, in which the alkali metal cations can be located, and which are extending in different crystallographic orientations dependent on the space group of the compound. All structures are highly condensed and provide distorted cube-like coordination environments for the larger embedded alkali cations, which arrange themselves as endless chains in the *vierer-ring*-channels. The degree of condensation is specified by the value  $\kappa$  describing the ratio of the ions involved into the tetrahedral backbone structure (Li, Si):O, and equals 1 for  $\text{UCr}_4\text{C}_4$ -type alkali lithosilicates.

Structural distinctions can be made between the compounds based on the different exact symmetries, leading to different space groups. In addition to that, it has proven useful to apply specific general molecular formula notations for some of the compounds, depending on how many different alkali metal cations occupy selected positions in the *vierer-ring*-channels. A possible classification based on the different space groups could look as follows:

#### 2.1.1. $P\bar{1}$ (no. 2)

Up to now, only one alkali lithosilicate appears in this group, which is  $\text{K}[\text{Li}_3\text{SiO}_4]$  (KLSO).<sup>[41]</sup> The compound can be described by the general formula  $A[\text{Li}_3\text{SiO}_4]$  ( $A = \text{alkali ion}$ ) and is able to accommodate only  $\text{K}^+$ -ions in its *vierer-ring* channels. The fact that it crystallizes in such a low symmetry triclinic space group can be attributed to the large  $\text{K}^+$  ions, leading to a widening and distortion of the lithosilicate framework and thus to a loss of symmetry. Notably, this compound is isotypical to the structure of the extremely narrow band emitting nitrido lithoaluminate SLA mentioned earlier.<sup>[7]</sup>

#### 2.1.2. $I4_1/a$ (no. 88)

This group includes the compounds  $\text{Na}[\text{Li}_3\text{SiO}_4]$  (NLSO),<sup>[43]</sup> as well as the isostructural representatives  $\text{NaK}_7[\text{Li}_3\text{SiO}_4]_8$ <sup>[51,52]</sup> and  $\text{LiK}_7[\text{Li}_3\text{SiO}_4]_8$ <sup>[79]</sup> to NLSO. Just like in the case of KLSO, only one ion species ( $\text{Na}^+$ ) is available for the population of the *vierer-ring* channels in NLSO. Thus, the general molecular formula  $A[\text{Li}_3\text{SiO}_4]$  applies here as well. The compounds  $\text{NaK}_7[\text{Li}_3\text{SiO}_4]_8$  and  $\text{LiK}_7[\text{Li}_3\text{SiO}_4]_8$ , on the other hand, can accommodate two different cations (Na and K or Li and K) in a fixed ratio of 1:7 inside the *vierer-ring* channels. For this reason, a general sum formula  $A_8[\text{Li}_3\text{SiO}_4]_8$  is used for these two. The compounds are a striking example that the incorporation of only one smaller alkali cation ( $\text{Na}^+$  or  $\text{Li}^+$ ) per eight KLSO units can already

induce structural change from a disordered triclinic  $P\bar{1}$  to the highly symmetric and ordered tetragonal  $I4_1/a$ -type structure.

#### 2.1.3. $C2/m$ (no. 12)

Typical representatives crystallizing in this monoclinic space group are  $\text{RbLi}[\text{Li}_3\text{SiO}_4]_2$ <sup>[44]</sup> and  $\text{RbNa}[\text{Li}_3\text{SiO}_4]_2$ .<sup>[45]</sup> Also here, two different alkali metal cations are located in the channels ( $\text{Rb}^+$  and  $\text{Na}^+$  or  $\text{Rb}^+$  and  $\text{Li}^+$ , respectively). In both compounds, the first *vierer-ring* channel is occupied by  $\text{Rb}^+$ . In the case of  $\text{RbNa}[\text{Li}_3\text{SiO}_4]_2$ , the second channel hosts  $\text{Na}^+$  in an eight-fold coordinated cube-like position, while  $\text{Li}^+$  in  $\text{RbLi}[\text{Li}_3\text{SiO}_4]_2$  occupies square planar coordinated positions between the, in this case, vacant cube-like coordination polyhedra. Furthermore, there is the compound  $\text{NaK}_2\text{Li}[\text{Li}_3\text{SiO}_4]_4$  crystallizing in this space group, which, adapting the molecular formula from the previous two compounds, can also be described as  $\text{KNa}_{0.5}\text{Li}_{0.5}[\text{Li}_3\text{SiO}_4]_2$ . Accordingly, the *vierer-ring* channel occupied by  $\text{Rb}^+$  in the first two compounds, contains  $\text{K}^+$  in this case. In the second channel, both  $\text{Na}^+$  in the cube-like coordination polyhedra and  $\text{Li}^+$  on the square planar coordinated positions are present with an occupation factor of 0.5 each.

#### 2.1.4. $I4/m$ (no. 87)

With a general formula  $A_4[\text{Li}_3\text{SiO}_4]_4$ , most of the  $\text{UCr}_4\text{C}_4$ -type alkali lithosilicates are included in this category and characterized by a higher variety of substitution possibilities in their channels. Up to four different alkali cations of varying size can occupy the *vierer-ring* channels oriented along the crystallographic  $c$  axis, of which two are occupied with the alkali-metal cations: The higher symmetric *vierer-ring* channel (CH1) is entirely confined by  $[\text{LiO}_4]^{7-}$  tetrahedra and, in all structures reported so far, accommodates two distinct cation sites usually occupied by the heavier cations. One coordination sphere is slightly larger than the other one, but both are eight-fold coordinated by equidistant oxide ions. The second *vierer-ring* channel (CH2) is confined by both  $[\text{LiO}_4]^{7-}$  and  $[\text{SiO}_4]^{4-}$  tetrahedra and generally provides a distorted eightfold cube-like coordination sphere. The third channel, also confined by  $[\text{LiO}_4]^{7-}$  and  $[\text{SiO}_4]^{4-}$  tetrahedra, remains unoccupied. A compilation of all presently known  $\text{Eu}^{2+}$ -activated alkali lithosilicates crystallizing in the tetragonal space group  $I4/m$  is summarized in **Table 1**. It is noteworthy that the lattice parameters are in a similar range for all compounds regardless of the exact composition. Obviously, cations of different size can occupy the *vierer-ring* channels without having a significant impact on the dimension of the rigid lithosilicate network. Consequently, the cell parameters and the powder diffraction patterns of the compounds are hardly discernable, which makes structural elucidations by means of, for example, Rietveld refinement in these compounds somewhat ambiguous. Single-crystal diffraction data of alkali lithosilicate phosphors are so far only provided for  $\text{RbKLi}_2[\text{Li}_3\text{SiO}_4]_4$ ,<sup>[21]</sup>  $\text{CsRbNaLi}[\text{Li}_3\text{SiO}_4]_4$ ,<sup>[56]</sup> and within this work, now also for “ $\text{K}_2\text{Na}_2[\text{Li}_3\text{SiO}_4]_4$ ”. For all the other phosphors, only powder diffraction data were used for the structural elucidation.<sup>[57]</sup> In the literature, the molecular

**Table 1.** List of all hitherto known alkali lithosilicate phosphors crystallizing in the tetragonal space group  $I4/m$  (no. 87) with eventually performed analyses and corresponding temperature: SCXRD or low-temperature luminescence measurements (LTL). “–” indicates no report on temperature/spectrum.

Eu <sup>2+</sup> -doped host structure	SCXRD		LTL		Ref.
	Yes/No	T [K]	Yes/No	T [K]	
“K <sub>2</sub> Na <sub>2</sub> [Li <sub>3</sub> SiO <sub>4</sub> ] <sub>4</sub> ”	No	–	Yes	80	[61]
RbKLi <sub>2</sub> [Li <sub>3</sub> SiO <sub>4</sub> ] <sub>4</sub>	Yes	173	No	–	[21]
CsRbNaLi[Li <sub>3</sub> SiO <sub>4</sub> ] <sub>4</sub>	Yes	293	No	–	[56]
RbNa <sub>3</sub> [Li <sub>3</sub> SiO <sub>4</sub> ] <sub>4</sub>	No	–	Yes	80	[58,59]
RbKNa <sub>2</sub> [Li <sub>3</sub> SiO <sub>4</sub> ] <sub>4</sub>	No	–	No	–	[55]
CsKNaLi[Li <sub>3</sub> SiO <sub>4</sub> ] <sub>4</sub>	No/No	–/–	Yes/No	10/–	[62,63]
CsKNa <sub>2</sub> [Li <sub>3</sub> SiO <sub>4</sub> ] <sub>4</sub>	No/No	–/–	No/Yes	–/75	[55,63]

formula “K<sub>2</sub>Na<sub>2</sub>[Li<sub>3</sub>SiO<sub>4</sub>]<sub>4</sub>” is often used, but our investigations suggest that this does not fully capture the structural details. Similar to RbKLi<sub>2</sub>[Li<sub>3</sub>SiO<sub>4</sub>]<sub>4</sub> and CsRbNaLi[Li<sub>3</sub>SiO<sub>4</sub>]<sub>4</sub>, Li<sup>+</sup> is present not only as a network building ion, but is also found in CH2. This is an important detail for the investigation of the compound, which is overlooked without SCXRD data and is not taken into account with the simplified molecular formula. In fact, previous literature on these alkali lithosilicate phosphors has hardly addressed the question of whether the channel CH2 can also host other ions besides Na<sup>+</sup>, although there are already clear indications in Hoppe’s first publications that this should be the case.<sup>[43]</sup> An especially challenging problem is the refinement or even proof of possible presence of the light Li<sup>+</sup> ions in CH2 from solely (averaged) PXRD data. Powder X-ray methods do not enable a resilient structural elucidation of such advanced problems, which is why a combined approach of SCXRD and high-resolution luminescence spectroscopy was selected to achieve a better understanding of structure-property relationships. The

high-resolution luminescence spectroscopy on incorporated Eu<sup>2+</sup> ions and their structurally sensitive excited 4f<sup>6</sup>5d<sup>1</sup> configuration allows a correlation of both the number and energies of the emission bands to the host structure and chemistry and thus, permits an assessment of the plausibility of the suggested structure models. Advanced transparent ligand-field calculations capable of treating excited states (unlike most DFT methods) finally offer an independent way to confirm the spectroscopic assignments. Such a feedback cycle of independent methods is mandatory to resolve and confirm such advanced structural problems and demonstrate the power that lies in a combined usage of single-crystal structure elucidation together with luminescence spectroscopy and selected theoretical approaches for this type of questions.<sup>[80–83]</sup>

## 2.2. Crystal Structure

Single-crystal structure refinements were conducted on cyan-emitting crystals obtained by the syntheses of “K<sub>2</sub>Na<sub>2</sub>[Li<sub>3</sub>SiO<sub>4</sub>]<sub>4</sub>:Eu<sup>2+</sup>” described in the Experimental Section. A single-crystal of particularly good quality ( $R\sigma = 1.78\%$ ;  $R_{\text{int}} = 2.50\%$ ;  $R_1$  (all data) = 2.04%) yielded lattice parameters of  $a = 10.9148(4)$  Å and  $c = 6.2508(2)$  Å. A structural model of the crystal with the found sum formula  $\text{K}_{1.586(8)}\text{Na}_{2.114(9)}\text{Li}_{0.300(4)}[\text{Li}_3\text{SiO}_4]_4$  (abbreviated as “K<sub>1.6</sub>Na<sub>2.1</sub>Li<sub>0.3</sub>[Li<sub>3</sub>SiO<sub>4</sub>]<sub>4</sub>:Eu<sup>2+</sup>”, or KNLLSO for better comparability with literature) is depicted in **Figure 1**.

In what follows, we compare our structural model from single-crystal diffraction data with the one reported earlier by Zhao et al. from Rietveld refinements on powdered samples of “Na<sub>0.5</sub>K<sub>0.5</sub>[Li<sub>3</sub>SiO<sub>4</sub>]:Eu<sup>2+</sup>” (NKLSO:Eu<sup>2+</sup>).<sup>[61]</sup> It should be noted that in this case, the refinement was carried out using RbNa<sub>3</sub>[Li<sub>3</sub>SiO<sub>4</sub>]<sub>4</sub> as structural input, by distributing K/Na as mixed ions on the three cation layers Rb, Na1, and Na2 and refining them. Already by the selection of these starting conditions, it becomes evident that Li<sup>+</sup> on the square planar

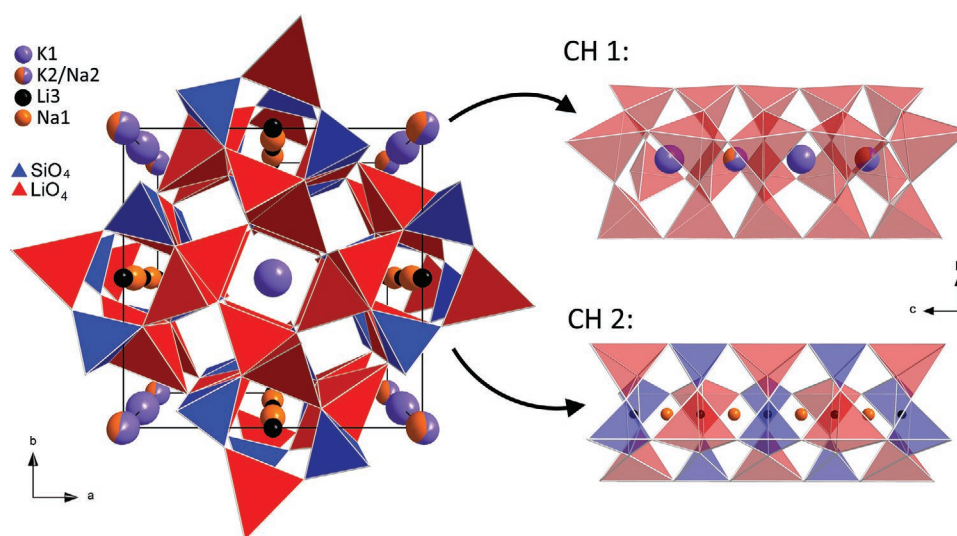


**Figure 1.** Structural model of KNLLSO according to single-crystal diffraction data. The two *vierer-ring*-channels filled with alkali metal ions are shown in detail, and in the case of CH2, the residual electron densities on the square planar coordinated positions are accounted for as Li<sup>+</sup> ions.

**Table 2.** Atomic coordinates and site-occupation factors (S.O.F.) of the cations in CH1 and CH2 in “ $\text{K}_2\text{Na}_2[\text{Li}_3\text{SiO}_4]_4$ ”,<sup>[61]</sup> comparing the original description and the results from the present publication.

	x y z	Atom	Zhao et al. (2019)	This work
			$\text{Na}_{0.58(4)}\text{K}_{0.42(4)}\text{Li}_3\text{SiO}_4$	$\text{K}_{1.582(8)}\text{Na}_{2.119(9)}\text{Li}_{0.299(4)}[\text{Li}_3\text{SiO}_4]_4$
			S.O.F.	S.O.F.
CH1:	0 0 ½	K	1	1
	0 0 0	K/Na	0.67(3)/0.33(3)	0.582(8)/0.418(8)
CH2:	0 ½ ¼	Na	1	0.850(4)
	0 ½ 0	Li		0.150(4)

coordinated positions cannot be considered in their later argumentation.

There are some similarities between our proposed structural model and the one reported by Zhao et al.<sup>[61]</sup> Like in all presently known alkali lithosilicates, the basic structure consists of a highly condensed tetrahedral network forming *vierer-ring* channels. Especially for the channel CH1 hosting the heavier alkali-metal ions, similar occupation factors, as expected, are given in both publications, as is summarized in **Table 2**. One of the two available eightfold coordinated cation sites in both cases is fully occupied with  $\text{K}^+$ . The other eightfold coordination polyhedron has a smaller volume and contains a randomly mixed occupation of  $\text{K}^+$  and  $\text{Na}^+$  ions. The ratios of K/Na are comparable, being 58.6(8)% to 41.4(8)% for KNLSO and 67(3)% to 33(3)% for NKLSO. Differences between our proposed model from single-crystal data and the one by Zhao et al. from powder-diffraction data are obvious in the occupation pattern of the

second channel CH2. Zhao et al. proposed a refinement with full  $\text{Na}^+$  occupation on the distorted cube-like position, while the  $\text{Li}^+$  ions are solely tetrahedrally coordinated and part of the network substructure.<sup>[61]</sup> There was no discussion of the possibility of a simultaneous presence of  $\text{Na}^+$  and  $\text{Li}^+$  within CH2 reported, although the respective analogs  $\text{CsKNaLi}[\text{Li}_3\text{SiO}_4]_4$ ,  $\text{RbKLi}_2[\text{Li}_3\text{SiO}_4]_4$ , and  $\text{CsRbNaLi}[\text{Li}_3\text{SiO}_4]_4$  clearly share that feature of mixed occupation in CH2, as was convincingly elucidated from single-crystal data.<sup>[21,45,56,62,63]</sup> For this reason, the data set was used to test a series of refinements based on different structural models to rank their accuracy. There are three main structural motifs regarding CH2 that can be considered, which are schematically depicted in **Figure 2**.

Refinement (a) refers to the structural model of Zhao et al.,<sup>[61]</sup> considering only  $\text{Na}^+$  in the center of the cube-like coordination polyhedra. This model serves as a reference point for the following refinements. In contrast to that, we assumed the

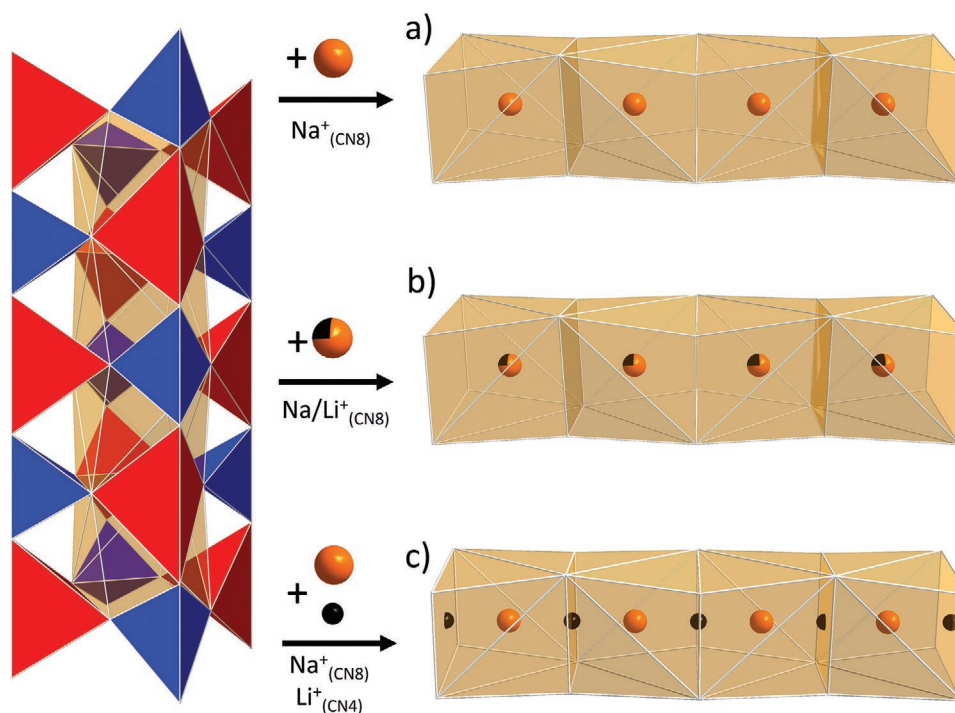


**Figure 2.** Three different models for the calculation of the occupancy in CH2. Model (a) is the refinement proposed in the structural model of Zhao et al. based on  $\text{RbNa}_3[\text{Li}_3\text{SiO}_4]_4$  as starting model,<sup>[45,61]</sup> model (b) additionally includes  $\text{Li}^+$  on the eight-fold coordinated site as a partially mixed  $\text{Na}^+/\text{Li}^+$ -occupation, and model (c) takes  $\text{Li}^+$  on the square planar coordinated site between the cube-like  $\text{Na}^+$ -polyhedra into account.

presence of both  $\text{Na}^+$  and  $\text{Li}^+$  in this channel in all our structural proposals on the basis of single-crystal structure data. However, it has been found that in the case of the consideration of exclusively  $\text{Na}^+$ , the site is underoccupied when the occupation factor is released. Therefore, in our first model (b), it was presumed that the  $\text{Na}^+$  sites in CH2 are mixed occupied with  $\text{Li}^+$  meaning that both ions are eight-fold coordinated in form of distorted cubes. For all investigated single-crystals, this resulted in an improvement of the  $R$  value by up to more than one percent at the final stage of the refinement compared to our refinement based on model (a), which is far beyond the usual improvement of  $R$  values by simply adding more parameters to the refinement. However, the cube-like coordination polyhedron would give rise to large Li–O distances and is practically not encountered for this small alkali ion in solids. An insightful example for that is the simple binary oxide  $\text{Li}_2\text{O}$  which crystallizes in an antifluorite-type structure with all  $\text{Li}^+$  ions located in the tetrahedral holes instead of the otherwise possible sites with cubic coordination. In that simple compound, for example, the Li–O distances are 1.996 Å.<sup>[84]</sup> This approximates the theoretically calculated distances of  $\text{Li}^+$  in tetrahedral coordination with oxygen of 1.97 Å. Refinement according to model (b) yields Li–O distances of 2.4585(6) and 2.7014(6) Å in an eightfold cube-like coordination, which is still quite high compared to a theoretically calculated value of 2.340 Å.

Moreover, the structural refinement leads to a significant unassigned residual electron density within CH2. It is located on the square planar faces of the cube-like coordination polyhedra and appears already in model (a) but is even more pronounced when refining by means of model (b). Out of that reason, we also considered another structural model to take the preference of  $\text{Li}^+$  ions for the small coordination number of 4 into account. Consequently, in the structural model (c),  $\text{Na}^+$  ions are located in the center of the cube-like coordination polyhedra, while  $\text{Li}^+$  ions are situated on the square planar faces of the cubes in between. The site occupation factor of all sites in CH2 was kept free and normalized to one, which resulted in a Na/Li ratio of 85.0(4)%/15.0(4)% in the case of the refined single-crystal in KNLLSO. Compared to model b), no significant changes in the  $R$  value were found but the Li–O bond

lengths are in a more common range.<sup>[85]</sup> This type of loading of CH2 is analogous to that of  $\text{CsRbNaLi}[\text{Li}_3\text{SiO}_4]_4\text{:Eu}^{2+}$ ,<sup>[56]</sup>  $\text{RbKLi}_2[\text{Li}_3\text{SiO}_4]_4\text{:Eu}^{2+}$ ,<sup>[21]</sup> and of  $\text{CsKNaLi}[\text{Li}_3\text{SiO}_4]_4\text{:Eu}^{2+}$ ,<sup>[45,62,63]</sup> with the single-crystal data of the latter already described by Hoppe. It is noteworthy that even their publication already deals with the question of how the filling of CH2 could look like in reality, as the authors correctly indicate that a simultaneously ordered occupation with  $\text{Na}^+$  and  $\text{Li}^+$  as depicted in Figure 2c is not very favorable due to the very short resulting Na–Li distances and the consequent repulsion. An alternative proposal by Hoppe et al. was the formation of distinct  $\text{Na}^+$  and  $\text{Li}^+$  domains alternating at unknown rates, resulting in vacancies at the domain boundaries (Figure 3).<sup>[45]</sup> However, it can be assumed that the domains must have an ordered lateral extension over a wider range since the presence of many domain boundaries results in a high number of defects, which destabilizes the crystal structure at ambient conditions. The domain boundaries and the related vacancies are also expected to play an important role in charge balancing in case of  $\text{Eu}^{2+}$  doping, as will be explained below. Overall, it is important to note that the structural models as depicted in Figure 2b,c, and Figure 3 are hardly distinguishable with “simple” X-ray diffraction, which only yields an averaged electron density distribution along CH2, especially if a light ion and weak X-ray scatterer such as  $\text{Li}^+$  is involved. This is particularly true for powder diffraction techniques, which suffer from the additional averaging effect over several crystallites thereby severely limiting the precision in the electron density distribution determination. The different structural models can be at least partially distinguished with higher accuracy in the case of a single-crystal based on a refinement and comparison of the resulting  $R$  values ( $R_1$  and  $wR_2$ ).

Thus, from the improved  $R$  values of the refinements based on single-crystal diffraction data and the comparison to the structurally well-studied analogs  $\text{CsKNaLi}[\text{Li}_3\text{SiO}_4]_4$ ,<sup>[45,62,63]</sup>  $\text{RbKLi}_2[\text{Li}_3\text{SiO}_4]_4\text{:Eu}^{2+}$ ,<sup>[21]</sup> and  $\text{CsRbNaLi}[\text{Li}_3\text{SiO}_4]_4\text{:Eu}^{2+}$ ,<sup>[56]</sup> the structural model as depicted in Figure 3 is the chemically most reasonable proposal consistent with the data. Taking this as an input for the refinement of the diffraction data of a high-quality single-crystal, we obtained a sum formula of  $\text{K}_{1.586(8)}\text{Na}_{2.114(9)}\text{Li}_{0.300(4)}[\text{Li}_3\text{SiO}_4]_4$  at final  $R$  values of  $R_1 = 1.83\%$  and  $wR_2 = 4.58\%$  (see

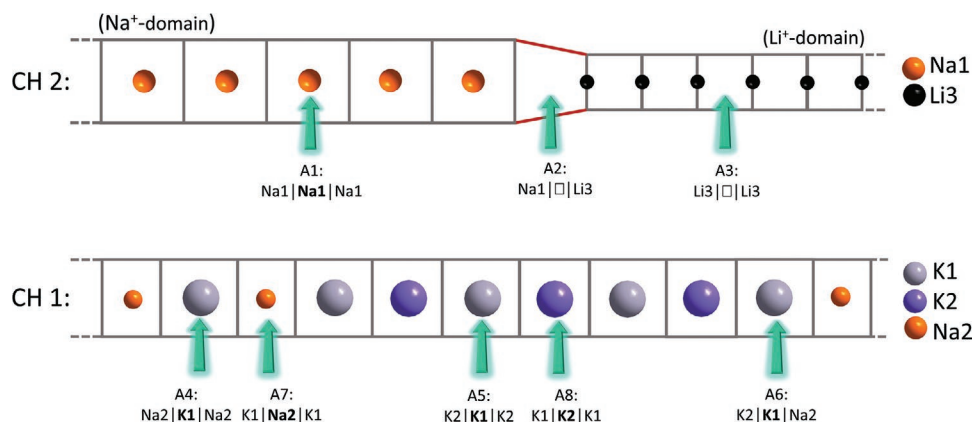


**Figure 3.** Schematic representation of the proposed real structure of the channels CH2 and CH1 (view perpendicular to the crystallographic  $c$  axis). The domain boundary in CH2 is marked in red introducing a vacancy between the  $\text{Na}^+$  and  $\text{Li}^+$  domains. The eight possible activator ion positions A1 to A8 are indicated with arrows, replacing the central ion (bold). Note that  $\text{Eu}^{2+}$  ions on positions A7 and A8 are spectroscopically indistinguishable due to the same coordination sphere (see text also).

single-crystal refinement in Table S1, Supporting Information). In order to confirm the representativeness of the refined single-crystal for the powder sample and to exclude the participation of secondary phases, additional Rietveld refinement was carried out (see Figure S1 and Table S2, Supporting Information) and also resulted in an excellent fit between structural input and resulting powder X-ray diffraction pattern with the experimental pattern.

According to the single-crystal refinement, Na<sup>+</sup> and Li<sup>+</sup> are present in CH2 in the statistical ratio 85 to 15, respectively, with Na–O bond lengths of 2.4585(6) Å and 2.7018(6) Å in an eight-fold coordinated cube-like environment, while the Li<sup>+</sup> ions are four-fold coordinated in a square planar setting with Li–O bond lengths of 1.8980(7) Å and 2.2040(7) Å. According to the Na/Li-ratio, it can be assumed that there is a higher number or that there are prolonged Na<sup>+</sup> domains compared to the Li<sup>+</sup> domains in the regarded single-crystal.

It can be assumed that the actual coordination polyhedra in the Na<sup>+</sup> domains are more expanded due to the larger cation radii, while the coordination spheres in the Li<sup>+</sup> domains tend to be smaller in the real structure. This issue is schematically depicted in Figure 3.

Doping with Eu<sup>2+</sup> thus gives rise to several possibilities for cation substitution, which are indicated by the cation positions in bold. Naturally, a structural relaxation occurs during the effective incorporation of Eu<sup>2+</sup> due to the different cation radii, which are not included in the representation. In CH2, it is possible to distinguish three different activator ion positions (indicated by arrows in Figure 3). The Eu<sup>2+</sup> ions could substitute Na<sup>+</sup> ions thus occupying an eight-fold coordinated site (A1). The second possibility is an occupation of the vacancy at the domain boundary (A2). Finally, Eu<sup>2+</sup> could be incorporated into a Li<sup>+</sup>-domain at the empty site in the center of the cube-like polyhedra (A3), which will require removal of two adjacent Li<sup>+</sup> in order to achieve charge neutrality, as we could recently show in the case of RbKLi<sub>2</sub>[Li<sub>3</sub>SiO<sub>4</sub>]<sub>4</sub>:Eu<sup>2+</sup> containing a purely Li-based channel CH2.<sup>[21]</sup> In CH1, an even higher number of distinguishable activator ion positions is expected in the real structure (see Figure 3). Initially, the question arises whether a domain formation could occur here as well with respect to the K2/Na2 site. In contrast to CH2, laterally extended domains at the K2/Na2 can be ruled out. Both the Na<sup>+</sup> and K<sup>+</sup> cations are solely located in the center of the cube-like coordination polyhedron due to their large sizes and are separated from each other by an additional K<sup>+</sup> ion at the fully ordered K1 sites. This spatial separation eliminates steric stress and the K2/Na2 sites are barely expected to influence each other. Therefore, the K1 position can effectively have three different environments for incorporated Eu<sup>2+</sup> ions: It can be surrounded by two adjacent Na<sup>+</sup> ions (A4), two adjacent K<sup>+</sup> ions (A5), or one adjacent K<sup>+</sup> and one adjacent Na<sup>+</sup> (A6) ion. In contrast, one may assume two possibilities for an occupation of the K2/Na2 site. However, due to the random distribution of these cations in CH1 together with the same cation environment by two adjacent K<sup>+</sup> ions on the K1 sites, occupation of the K2/Na2 site by Eu<sup>2+</sup> ions only results in one effective spectroscopically detectable doping site. Overall, the various cation environments in CH1 and CH2 result in totally seven distinguishable potential Eu<sup>2+</sup> doping sites.

Single-crystal structure data does not allow a precise statement about the actually occupied sites by Eu<sup>2+</sup> at the usually regarded low doping levels in phosphors (~1 mol%). In the investigated single-crystal however, no residual electron densities or over-/underoccupations were found, which would be an indicative feature for the presence of Eu<sup>2+</sup>.

### 2.3. High-Resolution Luminescence Spectroscopy of K<sub>1.6</sub>Na<sub>2.1</sub>Li<sub>0.3</sub>[Li<sub>3</sub>SiO<sub>4</sub>]<sub>4</sub>:Eu<sup>2+</sup> at 10 K

High-resolution photoluminescence spectroscopy can be a powerful tool to gain additional insights about the local structural environment of luminescent ions if their transitions are sensitive to structural effects. The proposed structural motifs according to the single-crystal structure determination should be reflected in the photoluminescence properties of Eu<sup>2+</sup>. Figure 4 depicts the luminescence spectra of K<sub>1.6</sub>Na<sub>2.1</sub>Li<sub>0.3</sub>[Li<sub>3</sub>SiO<sub>4</sub>]<sub>4</sub>:Eu<sup>2+</sup> (0.5 mol%) at 10 K.

At this temperature, emission band widths are minimized, which thereby improves the resolution of the luminescence spectra. Higher doped samples (5 mol% and 10 mol% Eu<sup>2+</sup>) were also investigated but do not reveal as well-resolved luminescence spectra due to inhomogeneous broadening. Moreover, energy transfer processes between Eu<sup>2+</sup> become more probable for higher doping fractions, and the (relative) emission intensities do not reflect the actual (relative) concentration of the Eu<sup>2+</sup> ions on a specific site. Finally, also luminescence decay curves become multi-exponential due to the interionic interaction. Overall, very dilute doping concentrations are advisable if luminescent ions are used as a structural probe.

Upon selective excitation in the ultraviolet (UV) or blue range, it is possible to detect up to seven resolved emission bands between 415 and 520 nm. This is in contrast to the findings by Zhao et al. who reported three emission bands in an 8 mol% Eu<sup>2+</sup>-activated sample of their proposed composition K<sub>2</sub>Na<sub>2</sub>[Li<sub>3</sub>SiO<sub>4</sub>]<sub>4</sub>.<sup>[61]</sup> It is important to note, however, that their spectra were only recorded at 80 K, which is still not sufficient to fully resolve all present emission bands (see Figure S2, Supporting Information, for temperature-dependent photoluminescence measurements).

The luminescence decay traces of all resolved emission bands were close to single exponential with decay times in the order of 0.4–1 μs and increase with the monitored emission wavelength (see Figure S3, Supporting Information). The μs range of the decay times clearly indicates that all emission bands have to be related to the presence of Eu<sup>2+</sup>,<sup>[86]</sup> while the single exponential behavior together with the photonically induced increase of the decay time  $\tau_{\text{rad}}$  with emission wavelength  $\lambda_{\text{em}}$  (ideally:  $\tau_{\text{rad}} \propto n |\chi(n)|^2 \lambda_{\text{em}}^3$ , with  $\chi(n)$  as a local field correction factor dependent on the refractive index of the host compound at the given wavelength  $\lambda_{\text{em}}$ <sup>[87,88]</sup>) indicate that the luminescence decay is purely radiative and excludes any energy transfer interactions among the different Eu<sup>2+</sup> ions at the low doping concentrations employed in our study. Overall, the combination of steady-state and time-resolved luminescence data at low measurement temperatures together with the very low doping concentration provides optimum conditions for an accurate resolution of the emission bands, and provides

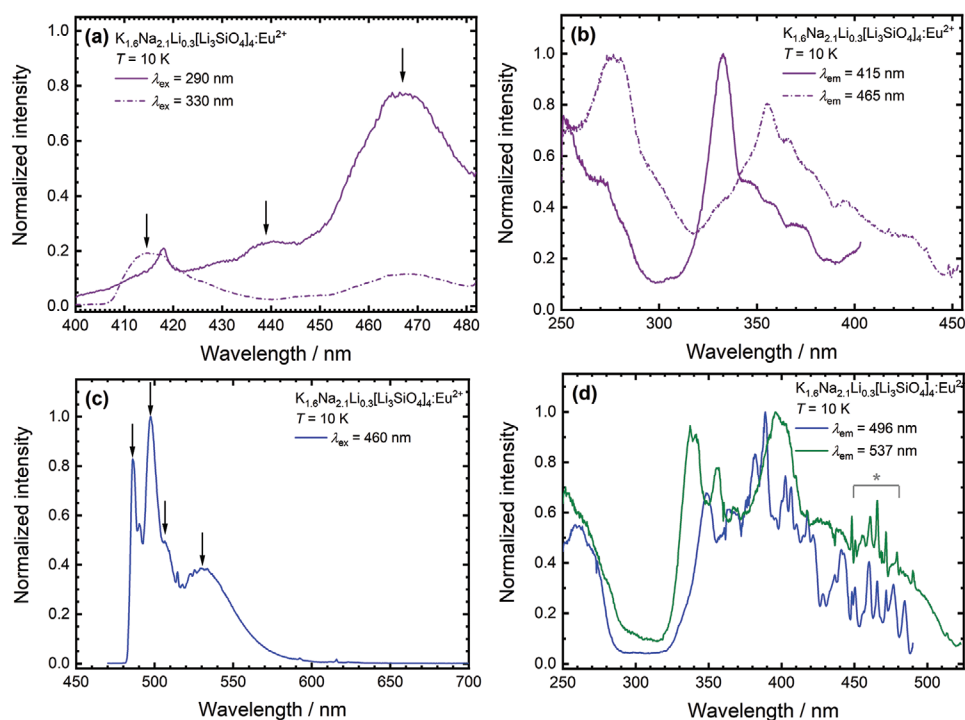


**Figure 4.** Photoluminescence emission and excitation spectra of  $\text{K}_{1.6}\text{Na}_{2.1}\text{Li}_{0.3}[\text{Li}_3\text{SiO}_4]_4:\text{Eu}^{2+}$  (0.5 mol%) at 10 K. a) Emission spectra in the violet and blue range due to  $\text{Eu}^{2+}$  on the K1 and K2/Na2 sites with b) corresponding excitation spectra. c) Emission spectrum in the cyan and green range with d) corresponding excitation spectra. Excitation and monitored emission wavelengths in each case are indicated, respectively. Arrows mark assigned emission bands, while unmarked peaks stem from vibronic fine structure (see text for detailed explanation). The range marked with an asterisk in the excitation spectra in d) indicates overlap with lines from the Xe lamp used as the excitation source.

additional information with respect to the earlier publication by Zhao et al.<sup>[61]</sup>

A more definite assignment of the different emission bands to the respective emitting  $\text{Eu}^{2+}$  centers in various crystallographic environments is possible by the parallel analysis of the photoluminescence excitation spectra upon detection of the various respective emission bands. The assignment follows simple crystal field theoretical arguments. The emission bands in the violet range relate to  $\text{Eu}^{2+}$  substituting the K atoms on the K1 site in the host compound. Given the large size of  $\text{K}^+$  with eight-fold coordination ( $r(\text{K}^+) = 1.51 \text{ \AA}$ ) compared to  $\text{Eu}^{2+}$  ( $r(\text{Eu}^{2+}) = 1.25 \text{ \AA}$ ),<sup>[89]</sup> the crystal field splitting of the 5d orbitals of  $\text{Eu}^{2+}$  is expectedly small due to the correspondingly larger Eu–O distances at the K sites. This is indeed observed in the excitation spectra upon monitoring of the emission bands in the violet and blue range (see Figure 4b), which display two groups of broad bands. These can be formally assigned to the  $e_g$  and  $t_{2g}$  states in an approximately cubic crystal field with effective splitting  $10Dq$ . It is, however, important to note that the real site symmetry of the K sites (and all other alkali cations in the crystal structure of the lithosilicate) is not perfectly cubic given the tetragonal space group of the crystal structure and thus, this assignment is only an approximation. If the  $\text{Eu}^{2+}$  ions substitute the  $\text{K}^+$  ions on the K1 site, the mixed occupation on the neighboring K2/Na2 site can lead to three distinguishable cation environments: Na2–Eu1–Na2 (A4 in Figure 3), K2–Eu1–K2 (A5 in Figure 3), or Na2–Eu1–K2 = K2–Eu1–Na2 (A6 in Figure 3).

The emission energies in the violet range are also in the expected range for  $4f^65d^1 \rightarrow 4f^7$  transitions of  $\text{Eu}^{2+}$  as a comparison to other  $\text{Eu}^{2+}$ -activated K-based fluorides with perovskite-analog structures reveals.<sup>[67–71]</sup> Nonetheless, substitution of K sites by  $\text{Eu}^{2+}$  is a generally rarely encountered phenomenon,<sup>[37,67–72]</sup> as was also pointed out by Fang et al.<sup>[65,73]</sup> An example of such a compound related to the presently discussed one is  $\text{RbKLi}_2[\text{Li}_3\text{SiO}_4]_4:\text{Eu}^{2+}$ . The compound shows blue emission at 474 nm and some of us speculated that it was either doping on the  $\text{Rb}^+$  or the  $\text{K}^+$  site in CH1 that is responsible for the luminescence.<sup>[21]</sup> In fact, doping on a pure  $\text{Rb}^+$  site is even less likely due to the large polyhedron volume, so the emission here should also originate preferentially from  $\text{Eu}^{2+}$  on the  $\text{K}^+$  site. Despite the analogous occupation of an eight-fold coordinated  $\text{K}^+$  site, the lower energetic cyan emission at 474 nm in  $\text{RbKLi}_2[\text{Li}_3\text{SiO}_4]_4:\text{Eu}^{2+}$  compared to the violet ones observed in  $\text{K}_{1.6}\text{Na}_{2.1}\text{Li}_{0.3}[\text{Li}_3\text{SiO}_4]_4:\text{Eu}^{2+}$  can be related to the smaller  $[\text{EuO}_8]^{14-}$  polyhedron volume and the respective shorter average Eu–O distances at the K sites. Indeed, consideration of the two  $\text{K}^+$  sites as activator ion positions reveals that they differ significantly in their polyhedral volume, which is  $33.4 \text{ \AA}^3$  for the K2 site in  $\text{RbKLi}_2[\text{Li}_3\text{SiO}_4]_4:\text{Eu}^{2+}$  and  $39.3 \text{ \AA}^3$  for K1 in  $\text{K}_{1.6}\text{Na}_{2.1}\text{Li}_{0.3}[\text{Li}_3\text{SiO}_4]_4:\text{Eu}^{2+}$  (see Table S3, Supporting Information). Interestingly, a similar blue emission like in  $\text{RbKLi}_2[\text{Li}_3\text{SiO}_4]_4:\text{Eu}^{2+}$  also appears in  $\text{CsRbNaLi}[\text{Li}_3\text{SiO}_4]_4:\text{Eu}^{2+}$  at 473 nm without the presence of  $\text{K}^+$ .<sup>[56]</sup> According to single-crystal measurements, the position corresponding to the  $\text{K}^+$  site in  $\text{RbKLi}_2[\text{Li}_3\text{SiO}_4]_4$  is occupied by both  $\text{Rb}^+$  and  $\text{Na}^+$  in a



ratio of 31.8(1):68.2(1) in CsRbNaLi[Li<sub>3</sub>SiO<sub>4</sub>]<sub>4</sub>. With this ratio, a calculated average ionic radius for “Rb<sup>+</sup>/Na<sup>+</sup>” of 1.40 Å results, which is slightly smaller than the ionic radius of K<sup>+</sup> in eight-fold coordination (1.51 Å).<sup>[89]</sup> The more expressive values of the polyhedron volume are close for the Rb2/Na1 site in CsRbNaLi[Li<sub>3</sub>SiO<sub>4</sub>]<sub>4</sub> (polyhedron volume 32.7 Å<sup>3</sup>) to the K2 polyhedron in RbKLi<sub>2</sub>[Li<sub>3</sub>SiO<sub>4</sub>]<sub>4</sub>:Eu<sup>2+</sup> (polyhedron volume 33.4 Å<sup>3</sup>) and support once again the assignment that the blue emission originates from Eu<sup>2+</sup> on that site (see Table S3, Supporting Information).

As already explained for the example of K<sub>1.6</sub>Na<sub>2.1</sub>Li<sub>0.3</sub>[Li<sub>3</sub>SiO<sub>4</sub>]<sub>4</sub>:Eu<sup>2+</sup>, a formation of domains in CH1 is unlikely, so that it can be assumed that there are indeed “average” coordination polyhedra for the Rb/Na site in the real structure of CsRbNaLi[Li<sub>3</sub>SiO<sub>4</sub>]<sub>4</sub>. This results from the relaxation of the local structure depending on the ionic radii of Rb<sup>+</sup>/Na<sup>+</sup> or Cs<sup>+</sup>/Rb<sup>+</sup> ions that are likewise randomly distributed on the neighboring positions. For such a comparative analysis and assignment of 4f<sup>6</sup>5d<sup>1</sup> → 4f<sup>7</sup>-related emission bands of Eu<sup>2+</sup>, only isotopic compounds among the alkali lithosilicates (see Section 2.1) can be meaningfully related to one another, for which also high-quality single-crystal data are available.

To additionally confirm the assignment of the violet bands, we performed simulations of the electronic structure of Eu<sup>2+</sup> occupying the K sites with different surroundings. DFT methods were used to relax the structure of the doped system. However, it is important to note that the electronic structure is not directly obtained from DFT or any other mean-field approach that cannot describe the different electronic configurations within a manifold, but from the complete diagonalization of the Hamiltonian of the 4f<sup>7</sup> and 4f<sup>6</sup>5d manifolds including mutual electron repulsion, ligand field, and spin-orbit interactions parametrized from DFT results (see Experimental Section for more details). From the energy difference between the lowest 4f<sup>6</sup>5d<sup>1</sup>-related state and the lowest 4f<sup>7</sup>-related state in our simulations, we can estimate an emission wavelength of 413 nm for Eu<sup>2+</sup> in position A5, 423 nm for position A6 and 451 nm for position A4 (see Figure 3). Although the simulations contain a complete, lower symmetry parametrization of the ligand field, we can estimate an effective value for 10Dq as the splitting between the lower and the higher 5d ligand field state to compare to the experimental data. We obtain effective values of 10Dq ≈ 7900 cm<sup>-1</sup> for the A4 site, 10Dq ≈ 6800 cm<sup>-1</sup> for the A5 site, and 10Dq ≈ 7200 cm<sup>-1</sup> for the A6 site. These results are in good agreement with the experimental data compiled in Table 3 as obtained from the photoluminescence excitation spectra, which reinforces the assignment of the violet bands to their respective doping sites. The deviations between theory and experiment are partially attributed to the lacking spectral resolution of the excitation spectra at 10 K that makes an accurate determination of the effective 10Dq value from the spectra difficult.

One additional very narrow emission band is observed in the cyan range at 486 nm with a vibronic side feature at 490 nm. Since the related excitation spectra are also characterized by two groups of bands with only small energy gap, this emission band is assigned to Eu<sup>2+</sup> ions on the K2/Na2 site. Although the K<sup>+</sup> and Na<sup>+</sup> ions are randomly distributed on this site, they do share the same cation coordination (i.e., K1 site), which results

**Table 3.** Characteristic spectroscopic values extracted from the photoluminescence emission and excitation spectra of K<sub>1.6</sub>Na<sub>2.1</sub>Li<sub>0.3</sub>[Li<sub>3</sub>SiO<sub>4</sub>]<sub>4</sub>:Eu<sup>2+</sup> at T = 10 K. The assigned environments refer to the notation depicted in Figure 3. Estimated errors in the determined effective 10Dq values are around ±500 cm<sup>-1</sup>. Calculated values of 10Dq are given in brackets where appropriate.

Assignment	λ <sub>em</sub> [nm]	Environment	fwhm [cm <sup>-1</sup> ]	Eff. 10Dq [cm <sup>-1</sup> ]
Eu <sup>2+</sup> on K1 site	415	A5	835	8100 (calc.: 6800)
	440	A6	– <sup>a)</sup>	– <sup>a)</sup> (calc.: 7200)
	465	A4	1120	9205 (calc.: 7900)
Eu <sup>2+</sup> on K2/Na2 site	486	A7 = A8	155	14 130
Eu <sup>2+</sup> on Na1/Li3 site	497	A1	330	15 345
	506	A2	395	
	530	A3	1660	

<sup>a)</sup>could not be accurately determined due to substantial spectral overlap.

in only one expected emission band upon occupation with Eu<sup>2+</sup>. If the average K–O (2.852 Å) or Na–O (2.719 Å) distances in the representatives containing solely purely K- or Na-based sites with cubic coordinative environments are taken to estimate a weighted average cation-oxygen distance for the K2/Na2 site (based on the refined occupation), the resulting distance (2.797 Å) is longer than the derived value from single-crystal diffraction data (2.726 Å).<sup>[45]</sup> This shorter distance (see also Table S3, Supporting Information) leads to certain degree of coordinative pressure at the K2/Na2 site upon occupation with Eu<sup>2+</sup>, which results in a stronger crystal field splitting (see also excitation spectra in Figure 4b,d) and consequently, an emission band in the cyan spectral range compared to the emission bands in the violet range assigned to the Eu<sup>2+</sup> ions on the more expanded K1 sites. This coordinative pressure is also reflected in the comparably low fwhm of the emission band in the cyan range compared to the emission bands in the violet range (see Table 3). The vibronic side feature at 490 nm is unusually broad (fwhm ≈ 145 cm<sup>-1</sup>), which is an additional consequence of the mixed occupation at the K2/Na2 site.

The emission band at 486 nm has a rather small fwhm of 155 cm<sup>-1</sup> or 20 meV (≈ 4 nm in the wavelength scale, see also Table 3). This is a well-known consequence of the cube-like coordination pattern around the Eu<sup>2+</sup> ions that is embedded in a condensed network of [SiO<sub>4</sub>]<sup>4-</sup> and [LiO<sub>4</sub>]<sup>7-</sup> tetrahedra.<sup>[7,13,90]</sup> Such a structural feature inhibits a substantial change of the Eu–O bond distance upon excitation from the non-bonding 4f<sup>7</sup> ground configuration to the lowest excited, slightly more bonding 4f<sup>6</sup>5d<sup>1</sup>(e<sub>g</sub>) configuration. The observed emission wavelengths and the respective assignment to the occupation of the K2/Na2 sites also agree with earlier findings.<sup>[56,58,59]</sup> It should be noted, however, that the observation of an additional vibronic side feature at 490 nm implies a strong zero-phonon line at 486 nm. In the context of this interpretation, the observed fwhm of 155 cm<sup>-1</sup> is still high compared to the usually observed very sharp vibronic lines as reported in, for example, MgF<sub>2</sub>:Eu<sup>2+</sup><sup>[91]</sup> or REPO<sub>4</sub>:Eu<sup>2+</sup> (RE = Y, Lu),<sup>[92]</sup> which can be ascribed to the mixed occupancy at the K2/Na2 site.

In the green range, three additional emission bands are observable, one of them with pronounced vibronic fine

structure (see Figure 4(c)). The corresponding excitation spectra upon monitoring of these emission bands again reveal two major groups of bands, which can be assigned to the excitation into the  $4f^65d^1(e_g)$  and  $4f^65d^1(t_{2g})$  configurations of  $\text{Eu}^{2+}$  in an approximately cubic environment. In the framework of this interpretation, the respective effective crystal-field splitting is then larger compared to the ones observed in the excitation spectra related to the cyan or violet-blue emission bands, respectively. These findings indicate that the corresponding  $\text{Eu}^{2+}$  ions occupy sites with short Eu–O distances and a correspondingly strong crystal field, which matches those found in channel CH2 containing the  $\text{Na}^+$  and  $\text{Li}^+$  ions.

The presence of three emission bands helps resolve the different structural possibilities as suggested by single-crystal X-ray diffraction. If we first assume structural model (b), referring to a mixed Na/Li position in CH1, the cube-like coordinated Na1/Li3 site does not appear suitable for doping with  $\text{Eu}^{2+}$ . Because of the large difference in ionic radii between  $\text{Li}^+$  and  $\text{Eu}^{2+}$  ( $r(\text{Li}^+) = 0.92 \text{ \AA}$  and  $r(\text{Eu}^{2+}) = 1.25 \text{ \AA}$  for a coordination number of 8),<sup>[89]</sup> the  $\text{Eu}^{2+}$  ions would only expectedly exclusively substitute the  $\text{Na}^+$  ions ( $r(\text{Na}^+) = 1.18 \text{ \AA}$  in eightfold coordination)<sup>[89]</sup> in the crystal structure, which then leads to three different emission bands based on the cation environment possibilities  $\text{Li3-Eu(1)-Li3}$ ,  $\text{Na1-Eu(1)-Na1}$ , or  $\text{Li3-Eu(1)-Na1}$ . This is already consistent with the observations in the luminescence spectrum. An occupation of the Li3 site is not probable given the additional presence of the Na1 sites with much more matching size for  $\text{Eu}^{2+}$  ions. It is, however, noteworthy that  $\text{Eu}^{2+}$  can occupy small sites with very small concentrations but usually only if there is no other alternative site present. Examples include rutile-type crystallizing  $\text{MgF}_2:\text{Eu}^{2+}$ ,<sup>[91]</sup> rocksalt-type  $\text{MgS}:\text{Eu}^{2+}$ ,<sup>[93,94]</sup> the  $\text{CsNiCl}_3$ -type haloperovskite derivatives  $\text{CsMgX}_3:\text{Eu}^{2+}$  ( $X = \text{Br}, \text{I}$ )<sup>[80,95]</sup> with a contrarily large  $\text{Cs}^+$  site ( $r(\text{Cs}^+) = 1.88 \text{ \AA}$  for twelve-fold coordination in that structure),<sup>[89]</sup> or the olivine-type crystallizing  $\text{LiMgPO}_4:\text{Eu}^{2+}$ ,<sup>[96]</sup> in which the slightly larger octahedrally coordinated Li sites are occupied by the  $\text{Eu}^{2+}$  ions. In all these cases, the doping concentration of  $\text{Eu}^{2+}$  was below 1 mol%. In contrast, the  $\text{Eu}^{2+}$  ions exclusively occupy the larger alkali sites in the fluorides  $\text{AMgF}_3:\text{Eu}^{2+}$  ( $A = \text{Na}, \text{K}, \text{Rb}$ ) with a correspondingly small crystal field splitting of the 5d orbitals in the excited  $4f^65d^1$  configuration, which even makes the observation of the otherwise rarely encountered narrow line  $4f^7 \leftrightarrow 4f^7$  luminescence of  $\text{Eu}^{2+}$  in the UV range possible.<sup>[67–71]</sup> Thus, substitution of comparably much smaller cations by  $\text{Eu}^{2+}$  in crystalline host compounds is a rather exceptional case, especially if there are larger cation sites present that could be occupied instead.

The alternating occupation pattern (see motif c) in Figure 3 with  $\text{Li}^+$  ions at the faces of the cubes in a square planar coordination would imply  $\text{Na}^+ - \text{Li}^+$  distances of only around  $1.6 \text{ \AA}$ , which is electrostatically highly unfavorable. Moreover, square planar coordinated  $\text{Li}^+$  ions are too small ( $r(\text{Li}^+) = 0.59 \text{ \AA}$  for fourfold coordination) to be substituted by  $\text{Eu}^{2+}$  ions. This would imply only substitution of the  $\text{Na}^+$  ions resulting in one additional emission band. That structural motif is incompatible with the observed number of  $\text{Eu}^{2+}$ -related emission bands.

The final suggested motif consists of ordered domains containing solely  $\text{Na}^+$  ions at the center of the oxygen-built cubes or square planar coordinated  $\text{Li}^+$  ions at the faces of the cubes (see

Figure 3, CH2). While  $\text{Eu}^{2+}$  simply substitutes the  $\text{Na}^+$  ions, they can also occupy the centers of the cubes in the  $\text{Li}^+$ -based domains introducing  $\text{Li}^+$  vacancies, that is, the cation environment reads  $\text{Li3-}\square\text{-Eu(1)-}\square\text{-Li3}$ . These emerging vacancies on the square planar coordinated  $\text{Li}^+$  position directly adjacent to the activator ion position are represented by “ $\square$ ” and result naturally from the Eu – Li distances, which are otherwise much too small. An analogous situation was reported by some of the authors earlier in the case of  $\text{RbKLi}_2[\text{Li}_3\text{SiO}_4]_4:\text{Eu}^{2+}$ ,<sup>[21]</sup> which contains a purely Li-based channel. The related  $\text{Eu}^{2+}$  emission band was reported to be in the green spectral range at around  $532 \text{ nm}$ , which also perfectly agrees with the lowest energetic emission band observed in  $\text{K}_{1.6}\text{Na}_{2.1}\text{Li}_{0.3}[\text{Li}_3\text{SiO}_4]_4$ . Finally, the  $\text{Eu}^{2+}$  ions can occupy the domain boundary between the Na- and Li-based channel. Overall, this structural motif of CH2 also consistently explains the number and wavelength of the emission bands in the cyan and green range. While luminescence spectroscopy does not readily allow to distinguish between the structural model of Figure 2b with a mixed occupied Li3/Na1 site and the model with two ordered Na- and Li-based domains and an intermediate domain boundary (see Figure 3), only the combination with SCXRD finally makes an elucidation of the latter motif as the overall consistent one with the experimental data possible.

The lowest energetic emission band also shows a pronounced vibronic fine structure (see Figure 5) with a progression of  $\Delta = (115 \pm 10) \text{ cm}^{-1}$ , in good agreement with recent findings on  $\text{NaK}_2\text{Li}[\text{Li}_3\text{SiO}_4]_4:\text{Eu}^{2+}$  ( $\Delta = 131 \text{ cm}^{-1}$ ).<sup>[65]</sup> The corresponding zero-phonon transition is located at  $506 \text{ nm}$ . The progression is higher compared to other reported examples of an observed vibronic progression in  $\text{Eu}^{2+}$ -based  $4f^65d^1 \rightarrow 4f^7$  emission bands in oxidic hosts such as  $\text{SrB}_4\text{O}_7:\text{Eu}^{2+}$  ( $\Delta = 85 \text{ cm}^{-1}$ )<sup>[97]</sup> and in a similar range to the progressions found in hydride perovskites like  $\text{LiMH}_3:\text{Eu}^{2+}$  ( $M = \text{Sr}, \text{Ba}$ ) with  $\Delta = 100 \text{ cm}^{-1}$ .<sup>[98,99]</sup> Since hydride ions are known to be strong  $\sigma$ -donor ligands,

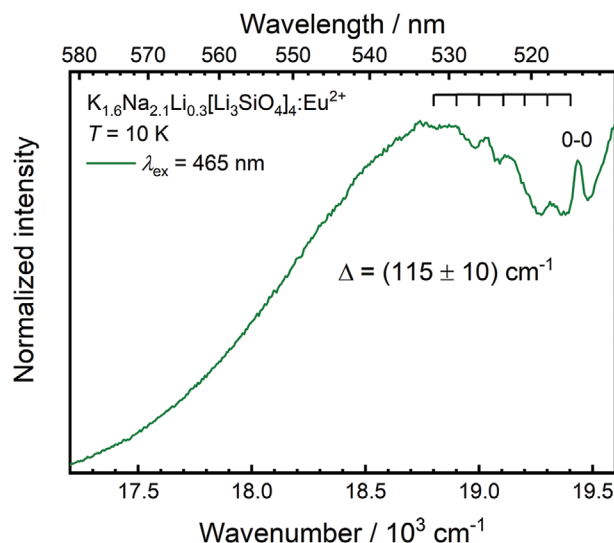


**Figure 5.** Vibronic fine structure of the emission band in the green spectral range of “ $\text{K}_{1.6}\text{Na}_{2.1}\text{Li}_{0.3}[\text{Li}_3\text{SiO}_4]_4:\text{Eu}^{2+}$ ” at 10 K stemming from  $\text{Eu}^{2+}$  in CH2 in the Li-based domain. The progression period in the emission spectrum is indicated.

the currently found vibronic progression on the green emission band in  $K_{1.6}Na_{2.1}Li_{0.3}[Li_3SiO_4]_4:Eu^{2+}$  indicates a strong and short Eu-O bond in the  $4f^7$  ground state. This finding additionally supports our assignment of  $Eu^{2+}$  in the vicinity of small  $Li^+$  ions, which induces short Eu-O bond distances. It is also consistent with the observations for both  $RbKLi_2[Li_3SiO_4]_4:Eu^{2+}$ <sup>[21]</sup> and  $CsRbNaLi[Li_3SiO_4]_4:Eu^{2+}$ ,<sup>[56]</sup> which all share the structural element of square planar coordinated  $Li^+$  in CH2 and which all show an emission in the green spectral region. A peculiar fine structure was also observed in the related excitation spectrum upon monitoring the green emission. However, due to significant overlap with overlaying lines of the Xe lamp and the additional superimposed fine structure that stems from the rich energy level landscape in the excited state configuration,<sup>[100,101]</sup> no accurate vibronic progression period could be extracted from the excitation spectrum (see also Figure 4d). Usually, a comparably higher value may be expected, however, due to a slightly more bonding nature of the Eu-O bonds in the lowest excited  $4f^65d^1(e_g)$  state based on experimental and theoretical findings on various divalent lanthanides in highly symmetric coordinative environments in solids.<sup>[74,102–105]</sup>

### 3. Conclusion

The  $Eu^{2+}$ -activated  $UCr_4C_4$ -type alkali lithosilicates are an emerging class of (ultra-)narrow band emitters to overcome the cyan gap and form the next generation of high color gamut LED phosphors for backlighting applications. In many of these compounds, a conventional structural elucidation with standard PXRD and Rietveld refinement does not give a complete picture of the cation distribution within the crystal structure, especially regarding the positions of the weakly scattering  $Li^+$  ions. In this work, we demonstrated how a combination of high-resolution photoluminescence spectroscopy at low-temperatures ( $T = 10$  K), structural refinement based on SCXRD, and ligand-field calculations allow to fully elucidate the non-trivial cation distribution in the alkali lithosilicates taking the compound  $K_{1.6}Na_{2.1}Li_{0.3}[Li_3SiO_4]_4:Eu^{2+}$  (0.5 mol%) as an example. SCXRD clearly suggests the presence of  $Li^+$  ions in both the backbone network of the  $[LiO_4]$  tetrahedra and within the cation channels, in contrast to previously reported findings based on structure refinements from solely powder-diffraction data. The new suggested structural model does not only fit perfectly well into the series of other isotypic  $UCr_4C_4$ -type alkali lithosilicates such as  $RbKLi_2[Li_3SiO_4]_4$  or  $CsRbNaLi[Li_3SiO_4]_4$ , but is also compatible with the high-resolution photoluminescence spectra at 10 K. Seven emission bands from the violet to green range are observable in  $K_{1.6}Na_{2.1}Li_{0.3}[Li_3SiO_4]_4:Eu^{2+}$  at 10 K that can be assigned to a  $4f^65d^1 \rightarrow 4f^7$  transition of  $Eu^{2+}$  occupying the various cation sites within the available two channels in the structure based on the related luminescence decay traces. Not only does this complement the findings from the SCXRD analysis but also reveals several unusual features. The observation of three emission bands in the violet and blue range indicates that the  $Eu^{2+}$  even substitute the large  $K^+$  ions, which is an otherwise rarely encountered phenomenon. High-level ligand field calculations with DFT-derived parameters on the  $4f^7$  ground and  $4f^65d^1$  excited configuration of  $Eu^{2+}$  independently confirmed this

assignment. These emission bands are only clearly resolved below 50 K. The other observable emission bands in the cyan and green range stem from  $Eu^{2+}$  ions within the cation channel containing mixed occupied  $K^+/Na^+$  or  $Li^+$  positions, respectively. From the number of emission bands, it could be elucidated that the cation channel composed of  $Na^+$  and  $Li^+$  is composed of domains containing solely cube-like coordinated  $Na^+$  or  $Li^+$  ions on the faces of the cubes. This structural pattern leads to an ultra-narrow  $Eu^{2+}$ -related emission band in the cyan range with a width of only  $155\text{ cm}^{-1}$  ( $20\text{ meV}$ ,  $\approx 4\text{ nm}$  in wavelength scale) at 10 K. The resulting insights into the origin of the emission bands fit well into the series of other  $UCr_4C_4$ -type alkali lithosilicates that show similar luminescence properties while featuring analogous structural motifs.

Several guidelines emerge out of this study. Our investigations showed once again that structure determination by means of single-crystal analysis is essential for the elucidation of the structure-property relationships in the alkali lithosilicates, since with PXRD important structural elements such as the  $Li^+$  positions and a resulting possible domain formation are not sufficiently well resolved. Although a precise description of the exact  $Li^+$  positions is still not trivial by means of X-ray diffraction, their consideration is essential for understanding the structure and the associated optical properties. Furthermore, it was shown that the establishment of appropriate structure-property relationships for the luminescence of  $Eu^{2+}$  requires low doping levels and low measurement temperatures to minimize broadening of the related emission bands in order to gain highest resolution and eliminate thermal quenching effects. The study on the alkali lithosilicate  $K_{1.6}Na_{2.1}Li_{0.3}[Li_3SiO_4]_4:Eu^{2+}$  is a textbook example for the powerful combination of SCXRD, low-temperature photoluminescence, and theoretical calculations to fully elucidate local structural details and exploit the local structural sensitivity of the  $4f^65d^1 \leftrightarrow 4f^7$  transition of  $Eu^{2+}$  in crystalline solids, which can be a guideline for the characterization of future phosphors.

### 4. Experimental Section

**Synthesis:** Powder samples with a nominal  $Eu^{2+}$ -concentration of 0.25 mol% were synthesized starting from  $Na_2CO_3$  (1.141 g, 0.0108 mol, Sigma Aldrich, 99.5%),  $K_2CO_3$  (1.480 g, 0.0107 mol, Alfa Aesar, 99%),  $Li_2CO_3$  (4.774 g, 0.0646 mol, Alfa Aesar, 99%),  $SiO_2$  (2.585 g, 0.0430 mol, Aerosil OX50 Evonik) and  $Eu_2O_3$  (0.019 g, 0.054 mmol, OSRAM Company). Potassium was formally substituted by Eu in this case.

Powder samples with a nominal  $Eu^{2+}$  concentration of 0.5 mol% were synthesized starting from  $Na_2CO_3$  (1.140 g, 0.01076 mol, Sigma Aldrich, 99.5%),  $K_2CO_3$  (1.471 g, 0.01064 mol, Alfa Aesar, 99%),  $Li_2CO_3$  (4.770 g, 0.0646 mol, Alfa Aesar, 99%),  $SiO_2$  (2.585 g, 0.0429 mol, Aerosil OX50 Evonik), and  $Eu_2O_3$  (0.038 g, 0.108 mmol, OSRAM Company). Potassium was formally substituted by Eu in this case.

The starting materials were mixed in a plastic bottle by using 10 ZrO<sub>2</sub> balls as a mixing and milling agent. The bottle was spun for 12 h on a rotating roll. The mixture was then transferred into an open Ni-crucible and positioned in a Nabertherm furnace (model LF120/14) flushed with forming gas ( $40\text{ L min}^{-1}$ ). The crucible was heated to  $1000\text{ }^\circ\text{C}$  ( $250\text{ }^\circ\text{C h}^{-1}$ ) and maintained at this temperature for 4 h and finally cooled down to room temperature within 6 h ( $\approx 162\text{ }^\circ\text{C h}^{-1}$ ). The product shows light blue to green color. The synthesis was optimized for single-crystal growth and the desired small fwhm of the cyan emission.

**Steady-State and Time-Resolved Photoluminescence Measurements:** All photoluminescence excitation and emission spectra were acquired on an

FLS920 Edinburgh Instruments spectrometer, equipped with a 450 W Xe lamp as the excitation source, a double Czerny-Turner excitation grating monochromator (0.22 m) blazed at 300 nm and a single Czerny-Turner emission monochromator (0.11 m) blazed at either 300 nm (for detection of the violet and blue emission bands) or 500 nm (for detection of the green emission bands). An R928 Hamamatsu photomultiplier tube was used as a detector. All spectra were corrected for lamp intensity, detector response, and grating efficiency. For cryogenic ( $T = 10$  K at sample) and temperature-dependent measurements below room temperature, the samples were cooled in an Oxford Instruments Liquid Flow He cryostat with an external temperature control unit. Luminescence decay measurements were also recorded on the same setup using a pulsed diode laser (405 nm, Edinburgh Instruments) as the excitation source and an H74220-60 photomultiplier as the detector. The time-resolved signal was detected using a time-correlated single-photon counting card (Edinburgh Instruments) connected to the photomultiplier.

**Single-crystal X-ray diffraction (SCXRD):** Crystallographic data of single-crystals of  $\text{K}_{1.6}\text{Na}_{2.1}\text{Li}_{0.3}[\text{Li}_3\text{SiO}_4]_4\text{Eu}^{2+}$  were obtained from a Bruker D8 Kappa X-ray diffractometer (Mo- $K_\alpha$  radiation,  $\lambda = 0.71073$  Å; Billerica, USA) equipped with a microfocus X-ray tube (Incoatec, Geesthacht, Germany) combined with a Photon II detector. Multi-scan absorption correction of the intensity data and data processing were conducted using the software tools SAINT<sup>[106]</sup> and SADABS.<sup>[107]</sup> The structure was solved using Direct Methods provided by SHELXS<sup>[108]</sup> and refined with SHELXL<sup>[109]</sup> as implemented in the WinGX suite.<sup>[110]</sup>

**Simulations:** DFT simulations were performed with the VASP code,<sup>[111,112]</sup> with the PAW method to reproduce the interaction between the valence and the core electrons.<sup>[113,114]</sup> The PBE approximation was used for the exchange-correlation potential.<sup>[115]</sup> Structural relaxation of a supercell containing 216 atoms with periodic boundary conditions was performed with a Hellmann-Feynman force convergence criterion of  $0.005$  eV Å<sup>-1</sup>. The complete  $4f^7$  and  $4f^65d$  manifolds of  $\text{Eu}^{2+}$  were obtained from a parameterized Hamiltonian including mutual electron repulsion, ligand field, and spin-orbit interaction.<sup>[76]</sup> Electron–electron and spin-orbit interactions were described via Slater–Condon and spin-orbit coupling parameters obtained from VASP with inclusion of the nephelauxetic effect. The ligand field part was extracted from the electronic wavefunctions and energy levels of the 4f and 5d states in VASP simulations with equal electronic occupation of each level to average their electron–electron interaction contribution. As DFT does not reproduce the electrostatic splitting between the 4f and 5d manifolds, a fixed shift was determined and kept fixed upon usage of the experimental emission wavelength of  $\text{Eu}^{2+}$  on the K2/Na2 site at 486 nm.

Further details of the crystal structure investigation may be obtained from the Fachinformationszentrum Karlsruhe, 76344 Eggenstein-Leopoldshafen (Germany), on quoting the depository number CSD-2098614.

## Supporting Information

Supporting Information is available from the Wiley Online Library or from the author.

## Acknowledgements

The authors would like to thank Dr. Frauke Philipp (OSRAM Opto Semiconductors GmbH) for preselection of suitable single crystals based on photoluminescence measurements.

Open access funding enabled and organized by Projekt DEAL.

## Conflict of Interest

The authors declare no conflict of interest.

## Data Availability Statement

Research data are not shared.

## Keywords

cyan gap,  $\text{Eu}^{2+}$ , high color gamut, light-emitting diodes,  $\text{UCr}_4\text{C}_4$ -type phosphors, ultra-narrow band emission

Received: August 9, 2021

Revised: August 26, 2021

Published online: October 8, 2021

- [1] R. Mueller-Mach, G. Mueller, M. R. Krames, H. A. Höpfe, F. Stadler, W. Schnick, T. Juestel, P. Schmidt, *Phys. Status Solidi A* **2005**, *202*, 1727.
- [2] R.-J. Xie, N. Hirosaki, *Sci. Technol. Adv. Mater.* **2007**, *8*, 588.
- [3] a) H. A. Höpfe, *Angew. Chem.* **2009**, *121*, 3626; b) H. A. Höpfe, *Angew. Chem., Int. Ed.* **2009**, *48*, 3572.
- [4] R.-J. Xie, N. Hirosaki, Y. Li, T. Takeda, *Materials* **2010**, *3*, 3777.
- [5] M. Zeuner, S. Pagano, W. Schnick, *Angew. Chem.* **2011**, *123*, 7898; *Angew. Chem., Int. Ed.* **2011**, *50*, 7754.
- [6] C. C. Lin, R.-S. Liu, *J. Phys. Chem. Lett.* **2011**, *2*, 1268.
- [7] P. Pust, V. Weiler, C. Hecht, A. Tücks, A. S. Wochnik, A.-K. Henß, D. Wiechert, C. Scheu, P. J. Schmidt, W. Schnick, *Nat. Mater.* **2014**, *13*, 891.
- [8] C. C. Lin, A. Meijerink, R.-S. Liu, *J. Phys. Chem. Lett.* **2016**, *7*, 495.
- [9] Z. Xia, Q. Liu, *Prog. Mater. Sci.* **2016**, *84*, 59.
- [10] J. L. Leão, M.-H. Fang, R.-S. Liu, *ECS J. Solid State Sci. Technol.* **2018**, *7*, R3111.
- [11] M. Zhao, Q. Zhang, Z. Xia, *Acc. Mater. Res.* **2020**, *1*, 137.
- [12] N. Hirosaki, R.-J. Xie, K. Kimoto, T. Sekiguchi, Y. Yamamoto, T. Suehiro, M. Mitomo, *Appl. Phys. Lett.* **2005**, *86*, 211905.
- [13] G. J. Hoerder, M. Seibald, D. Baumann, T. Schröder, S. Peschke, P. C. Schmid, T. Tyborski, P. Pust, I. Stoll, M. Bergler, C. Patzig, S. Reißaus, M. Krause, L. Berthold, T. Höche, D. Johrendt, H. Huppertz, *Nat. Commun.* **2019**, *10*, 1824.
- [14] M.-H. Fang, J. L. Leão, R.-S. Liu, *ACS Energy Lett.* **2018**, *3*, 2573.
- [15] P. Pust, P. J. Schmidt, W. Schnick, *Nat. Mater.* **2015**, *14*, 454.
- [16] J. Cho, J. H. Park, J. K. Kim, E. F. Schubert, *Laser Photonics Rev.* **2017**, *11*, 1600147.
- [17] M. Suta, J. George, *Nachr. Chem.* **2020**, *68*, 54.
- [18] X. Luo, R.-J. Xie, *J. Rare Earths* **2020**, *38*, 464.
- [19] A. G. Bispo-Jr, L. F. Saraiva, S. A. Lima, A. M. Pires, M. R. Davolos, *J. Lumin.* **2021**, *237*, 118167.
- [20] M. A. van de Haar, M. Tachikirt, A. C. Berends, M. R. Krames, A. Meijerink, F. T. Rabouw, *ACS Photonics* **2021**, *8*, 1784.
- [21] D. Dutzler, M. Seibald, D. Baumann, F. Philipp, S. Peschke, H. Huppertz, *Z. Naturforsch. B* **2019**, *74*, 535.
- [22] P. Pust, A. S. Wochnik, E. Baumann, P. J. Schmidt, D. Wiechert, C. Scheu, W. Schnick, *Chem. Mater.* **2014**, *26*, 3544.
- [23] H. Huppertz, W. Schnick, *Acta Crystallogr., Sect. C: Struct. Chem.* **1997**, *53*, 1751.
- [24] H. A. Höpfe, H. Lutz, P. Morys, W. Schnick, A. Seilmeier, *J. Phys. Chem. Solids* **2000**, *61*, 2001.
- [25] Y. Oyama, O. Kamigaito, *Jpn. J. Appl. Phys.* **1971**, *10*, 1637.
- [26] K. H. Jack, W. I. Wilson, *Nat. Phys. Sci.* **1972**, *238*, 28.
- [27] Y. Q. Li, A. C. A. Delsing, G. de With, H. T. Hintzen, *Chem. Mater.* **2005**, *17*, 3242.
- [28] H. A. Höpfe, F. Stadler, O. Oeckler, W. Schnick, *Angew. Chem.* **2004**, *116*, 5656; *Angew. Chem., Int. Ed.* **2004**, *43*, 5540.

- [29] O. Oeckler, F. Stadler, T. Rosenthal, W. Schnick, *Solid State Sci.* **2007**, 9, 205.
- [30] J. A. Kechele, O. Oeckler, F. Stadler, W. Schnick, *Solid State Sci.* **2009**, 11, 537.
- [31] Y. Q. Li, K. V. Ramanujachary, S. E. Lofland, G. de With, H. T. Hintzen, *J. Mater. Res.* **2006**, 21, 396.
- [32] F. Stadler, O. Oeckler, H. A. Höpfe, M. H. Möller, R. Pöttgen, B. D. Mosel, P. Schmidt, V. Duppel, A. Simon, W. Schnick, *Chem. - Eur. J.* **2006**, 12, 6984.
- [33] V. Bachmann, T. Jüstel, A. Meijerink, C. Ronda, P. J. Schmidt, *J. Lumin.* **2006**, 121, 441.
- [34] V. Bachmann, C. Ronda, O. Oeckler, W. Schnick, A. Meijerink, *Chem. Mater.* **2009**, 21, 316.
- [35] a) M. Seibald, O. Oeckler, V. R. Celinski, P. J. Schmidt, A. Tücks, W. Schnick, *Solid State Sci.* **2011**, 13, 1769; b) M. Seibald, T. Rosenthal, O. Oeckler, F. Fahrnbauer, A. Tücks, P. J. Schmidt, W. Schnick, *Chem. - Eur. J.* **2012**, 18, 13446; c) M. Seibald, T. Rosenthal, O. Oeckler, C. Maak, A. Tücks, P. J. Schmidt, D. Wiechert, W. Schnick, *Chem. Mater.* **2013**, 25, 1852; d) M. Seibald, T. Rosenthal, O. Oeckler, W. Schnick, *Crit. Rev. Solid State Mater. Sci.* **2014**, 39, 215.
- [36] N. Kunkel, H. Kohlmann, A. Sayede, M. Springborg, *Inorg. Chem.* **2011**, 50, 5873.
- [37] J. Ueda, T. Wylezich, N. Kunkel, S. Tanabe, *J. Mater. Chem. C* **2020**, 8, 5124.
- [38] P. M. Jaffe, E. Banks, *J. Electrochem. Soc.* **1955**, 102, 518.
- [39] N. Yamashita, I. Yamamoto, K. Ninagawa, T. Wada, Y. Yamashita, Y. Nakao, *Jpn. J. Appl. Phys.* **1985**, 24, 1174.
- [40] A. Meijerink, *Sci. China Mater.* **2019**, 62, 146.
- [41] R. Werthmann, R. Hoppe, *Z. Anorg. Allg. Chem.* **1984**, 509, 7.
- [42] R. Hofmann, B. Nowitzki, R. Hoppe, *Z. Naturforsch. B* **1985**, 40, 1441.
- [43] B. Nowitzki, R. Hoppe, *Rev. Chim. Miner.* **1986**, 23, 217.
- [44] K. Bernet, R. Hoppe, *Z. Anorg. Allg. Chem.* **1991**, 592, 93.
- [45] J. Hofmann, R. Brandes, R. Hoppe, *Z. Anorg. Allg. Chem.* **1994**, 620, 1495.
- [46] P. Strobel, C. Maak, V. Weiler, P. J. Schmidt, W. Schnick, *Angew. Chem.* **2018**, 130, 8875; *Angew. Chem., Int. Ed.* **2018**, 57, 8739.
- [47] P. Strobel, T. de Boer, V. Weiler, P. J. Schmidt, A. Moewes, W. Schnick, *Chem. Mater.* **2018**, 30, 3122.
- [48] E. Elzer, R. Niklaus, P. J. Strobel, V. Weiler, P. J. Schmidt, W. Schnick, *Chem. Mater.* **2019**, 31, 3174.
- [49] M. R. Amin, E. Elzer, W. Schnick, A. Moewes, *J. Phys. Chem. C* **2021**, 125, 11828.
- [50] M. Seibald, D. Baumann, T. Fiedler, S. Lange, H. Huppertz, D. Dutzler, T. Schröder, D. Bichler, G. Plundrich, S. Peschke, G. Hoerder, G. Achraimer, K. Wurst, WO 2018/029299 A1, **2017**.
- [51] D. Dutzler, M. Seibald, D. Baumann, H. Huppertz, *Angew. Chem.* **2018**, 130, 13865.
- [52] D. Dutzler, M. Seibald, D. Baumann, H. Huppertz, *Angew. Chem., Int. Ed.* **2018**, 57, 13676.
- [53] M. Iwaki, S. Kumagai, S. Konishi, A. Koizumi, T. Hasegawa, K. Uematsu, A. Itadani, K. Toda, M. Sato, *J. Alloys Compd.* **2019**, 776, 1016.
- [54] H. Liao, M. Zhao, Y. Zhou, M. S. Molokeev, Q. Liu, Q. Zhang, Z. Xia, *Adv. Funct. Mater.* **2019**, 29, 1901988.
- [55] M. Zhao, Y. Zhou, M. S. Molokeev, Q. Zhang, Q. Liu, Z. Xia, *Adv. Opt. Mater.* **2019**, 7, 1801631.
- [56] F. Ruegenberg, M. Seibald, D. Baumann, S. Peschke, P. C. Schmid, H. Huppertz, *Chem. - Eur. J.* **2020**, 26, 2204.
- [57] M. Seibald, D. Baumann, T. Fiedler, S. Lange, H. Huppertz, D. Dutzler, T. Schröder, D. Bichler, G. Plundrich, S. Peschke, G. Hoerder, G. Achraimer, K. Wurst, WO/2018/029304, **2018**.
- [58] H. Liao, M. Zhao, M. S. Molokeev, Q. Liu, Z. Xia, *Angew. Chem.* **2018**, 130, 11902.
- [59] H. Liao, M. Zhao, M. S. Molokeev, Q. Liu, Z. Xia, *Angew. Chem., Int. Ed.* **2018**, 57, 11728.
- [60] M. Zhao, H. Liao, L. Ning, Q. Zhang, Q. Liu, Z. Xia, *Adv. Mater.* **2018**, 30, 1802489.
- [61] M. Zhao, H. Liao, M. S. Molokeev, Y. Zhou, Q. Zhang, Q. Liu, Z. Xia, *Light: Sci. Appl.* **2019**, 8, 38.
- [62] L. Wang, X. Kong, P. Li, W. Ran, X. Lan, Q. Chen, J. Shi, *Inorg. Chem. Front.* **2019**, 6, 3604.
- [63] W. Wang, M. Tao, Y. Liu, Y. Wei, G. Xing, P. Dang, J. Lin, G. Li, *Chem. Mater.* **2019**, 31, 9200.
- [64] M.-H. Fang, P.-Y. Chen, Z. Bao, N. Majewska, T. Leśniewski, S. Mahlik, M. Grinberg, H.-S. Sheu, J.-F. Lee, R.-S. Liu, *J. Phys. Chem. Lett.* **2020**, 11, 6621.
- [65] M.-H. Fang, C. O. M. Mariano, K.-C. Chen, J.-C. Lin, Z. Bao, S. Mahlik, T. Lesniewski, K.-M. Lu, Y.-R. Lu, Y.-J. Wu, H.-S. Sheu, J.-F. Lee, S.-F. Hu, R.-S. Liu, J. P. Attfield, *Chem. Mater.* **2021**, 33, 1893.
- [66] M. Zhao, Z. Yang, L. Ning, Z. Xia, *Adv. Mater.* **2021**, 33, 2101428.
- [67] N. S. Altshuler, S. L. Korableva, L. D. Livanova, A. L. Stolov, *Sov. Phys. Solid State* **1974**, 15, 2155.
- [68] N. S. Altshuler, L. D. Livanova, A. L. Stolov, *Opt. Spectrosc.* **1974**, 36, 72.
- [69] R. Alcala, D. K. Sardar, W. A. Sibley, *J. Lumin.* **1982**, 27, 273.
- [70] A. Ellens, A. Meijerink, G. Blasse, *J. Lumin.* **1994**, 59, 293.
- [71] A. Ellens, A. Meijerink, G. Blasse, *J. Lumin.* **1994**, 60–61, 70.
- [72] N. Kunkel, A. Meijerink, M. Springborg, H. Kohlmann, *J. Mater. Chem. C* **2014**, 2, 4799.
- [73] M.-H. Fang, C. O. M. Mariano, P.-Y. Chen, S.-F. Hu, R.-S. Liu, *Chem. Mater.* **2020**, 32, 1748.
- [74] H. Ramanantoanina, F. Cimpoesu, C. Göttel, M. Sahnoun, B. Herden, M. Suta, C. Wickleder, W. Urland, C. Daul, *Inorg. Chem.* **2015**, 54, 8319.
- [75] C. Bulloni, A. García-Fuente, W. Urland, C. Daul, *Phys. Chem. Chem. Phys.* **2015**, 17, 24925.
- [76] A. García-Fuente, F. Baur, F. Cimpoesu, A. Vega, T. Jüstel, W. Urland, *Chem. - Eur. J.* **2018**, 24, 16276.
- [77] D. Böhnisch, J. Rosenboom, A. García-Fuente, W. Urland, T. Jüstel, F. Baur, *J. Mater. Chem. C* **2019**, 7, 6012.
- [78] F. Liebau, *Structural Chemistry of Silicates*, Springer, Berlin **1985**.
- [79] D. S. Wimmer, M. Seibald, D. Baumann, S. Peschke, K. Wurst, G. Heymann, D. Dutzler, A. Garcia-Fuente, W. Urland, H. Huppertz, **2021**.
- [80] M. Suta, C. Wickleder, *J. Mater. Chem. C* **2015**, 3, 5233.
- [81] T. Wylezich, S. Welinski, M. Hoelzel, P. Goldner, N. Kunkel, *J. Mater. Chem. C* **2018**, 6, 13006.
- [82] T. Wylezich, A. D. Sontakke, V. Castaing, M. Suta, B. Viana, A. Meijerink, N. Kunkel, *Chem. Mater.* **2019**, 31, 8957.
- [83] A. Mutschke, T. Wylezich, A. D. Sontakke, A. Meijerink, M. Hoelzel, N. Kunkel, *Adv. Opt. Mater.* **2021**, 9, 2002052.
- [84] J. Bijvoet, A. Claasen, A. Karssen, *Proc. K. Akad. Van Wet. Te Amst* **1926**, 29, 1286.
- [85] N. Wiberg, E. Wiberg, A. Hollemann, *Lehrbuch der Anorganischen Chemie*, de Gruyter, Berlin **2007**.
- [86] S. H. M. Poort, A. Meyerink, G. Blasse, *J. Phys. Chem. Solids* **1997**, 58, 1451.
- [87] D. Toptygin, *J. Fluoresc.* **2003**, 13, 201.
- [88] F. T. Rabouw, S. A. den Hartog, T. Senden, A. Meijerink, *Nat. Commun.* **2014**, 5, 3610.
- [89] R. D. Shannon, *Acta Crystallogr., Sect. A: Found. Adv.* **1976**, 32, 751.
- [90] S. Schmiechen, H. Schneider, P. Wagatha, C. Hecht, P. J. Schmidt, W. Schnick, *Chem. Mater.* **2014**, 26, 2712.
- [91] S. Lizzo, A. H. Velders, A. Meijerink, G. J. Dirksen, G. Blasse, *J. Lumin.* **1996**, 65, 303.
- [92] J. Zeler, M. Sulollari, A. Meijerink, M. Bettinelli, E. Zych, *J. Alloys Compd.* **2020**, 844, 156096.

- [93] S. Asano, Y. Nakao, *J. Phys. C: Solid State Phys.* **1979**, 12, 4095.
- [94] Y. Nakao, *J. Phys. Soc. Jpn.* **1980**, 48, 534.
- [95] M. Suta, P. Larsen, F. Lavoie-Cardinal, C. Wickleder, *J. Lumin.* **2014**, 149, 35.
- [96] S. Zhang, Y. Huang, L. Shi, H. J. Seo, *J. Phys.: Condens. Matter* **2010**, 22, 235402.
- [97] A. Meijerink, J. Nuyten, G. Blasse, *J. Lumin.* **1989**, 44, 19.
- [98] N. Kunkel, A. Meijerink, H. Kohlmann, *Phys. Chem. Chem. Phys.* **2014**, 16, 4807.
- [99] G. Lefevre, A. Herfurth, H. Kohlmann, A. Sayede, T. Wylezich, S. Welinski, P. Duarte Vaz, S. F. Parker, J. F. Blach, P. Goldner, N. Kunkel, *J. Phys. Chem. C* **2018**, 122, 10501.
- [100] H. A. Weakliem, *Phys. Rev. B* **1972**, 6, 2743.
- [101] J. J. Joos, P. F. Smet, L. Seijo, Z. Barandiarán, *Inorg. Chem. Front.* **2020**, 7, 871.
- [102] Z. Barandiarán, L. Seijo, *J. Chem. Phys.* **2003**, 119, 3785.
- [103] J. L. Pascual, Z. Barandiarán, L. Seijo, *Phys. Rev. B* **2007**, 76, 104109.
- [104] a) S. Mahlik, M. Grinberg, L. Shi, H. J. Seo, *J. Phys.: Condens. Matter* **2009**, 21, 235603; b) S. Mahlik, K. Wiśniewski, M. Grinberg, R. S. Meltzer, *J. Phys.: Condens. Matter* **2009**, 21, 245601.
- [105] M. de Jong, D. Biner, K. W. Krämer, Z. Barandiarán, L. Seijo, A. Meijerink, *J. Phys. Chem. Lett.* **2016**, 7, 2730.
- [106] BrukerSAINT, Bruker AXS Inc., Madison, Wisconsin **2014**.
- [107] L. Krause, R. Herbst-Irmer, G. M. Sheldrick, D. Stalke, *J. Appl. Crystallogr.* **2015**, 48, 3.
- [108] G. M. Sheldrick, *Acta Crystallogr., Sect. A: Found. Adv.* **2008**, 64, 112.
- [109] G. M. Sheldrick, *Acta Crystallogr., Sect. C: Struct. Chem.* **2015**, 71, 3.
- [110] L. J. Farrugia, *J. Appl. Crystallogr.* **2012**, 45, 849.
- [111] G. Kresse, J. Hafner, *Phys. Rev. B* **1993**, 47, 558.
- [112] G. Kresse, J. Furthmüller, *Phys. Rev. B* **1996**, 54, 11169.
- [113] P. E. Blöchl, *Phys. Rev. B* **1994**, 50, 17953.
- [114] G. Kresse, D. Joubert, *Phys. Rev. B* **1999**, 59, 1758.
- [115] J. P. Perdew, K. Burke, M. Ernzerhof, *Phys. Rev. Lett.* **1996**, 77, 3865.